Production cross sections of new neutron-rich isotopes with $Z = 92$–106 in the multinucleon transfer reaction ^{197}Au + ^{232}Th

Yu-Hai Zhang,[1,2] Jing-Jing Li,[2] Na Tang,[1,2] Xin-Rui Zhang,[3] Zhong Liu,[4] and Feng-Shou Zhang[1,2,5,*]

[1]*The Key Laboratory of Beam Technology of Ministry of Education, College of Nuclear Science and Technology, Beijing Normal University, Beijing 100875, China*

[2]*Institute of Radiation Technology, Beijing Academy of Science and Technology, Beijing 100875, China*

[3]*Department of Physics, Guangxi Normal University, Guilin 541004, China*

[4]*Institute of Modern Physics, Chinese Academy of Sciences, Lanzhou 730000, China*

[5]*Center of Theoretical Nuclear Physics, National Laboratory of Heavy Ion Accelerator of Lanzhou, Lanzhou 730000, China*

(Received 28 November 2022; accepted 2 February 2023; published 10 February 2023)

The multinucleon transfer reactions ^{197}Au + ^{232}Th, ^{186}W + ^{232}Th, and ^{238}U + ^{232}Th are investigated within the framework of dinuclear system (DNS) model with a decay model GEMINI++. The calculated isotopic production cross sections in the ^{136}Xe + ^{249}Cf reaction at $E_{\mathrm{c.m.}} = 567$ MeV can reproduce the experimental data well. Due to the subshell closures, the behavior of "inverse" quasifission process is found in the collisions of ^{186}W + ^{232}Th and ^{197}Au + ^{232}Th. The reaction ^{197}Au + ^{232}Th is more advantageous to produce neutron-rich isotopes with $Z =$ 92–106 than ^{186}W + ^{232}Th and ^{238}U + ^{232}Th, because it has the lowest value of the potential energy that needed to overcome in the nucleon transfer process. Furthermore, the incident energy dependence of isotopic production cross sections in the reaction ^{197}Au + ^{232}Th is studied. It is found that $E_{\mathrm{c.m.}} = 756.47$ MeV is more suitable for producing new isotopes with $Z = 92$–98, while $E_{\mathrm{c.m.}} = 690.69$ MeV is the optimal incident energy for $Z =$ 99–106. The effect of incident energy on the interaction time is also investigated. The production cross sections of 88 unknown neutron-rich transuranium nuclei are predicted with the cross sections at the order of 10^{-6} to 10 μb.

DOI: 10.1103/PhysRevC.107.024604

I. INTRODUCTION

Heavy nuclear collision associated with large mass transfer between reaction partners is a current frontier topic, which is crucial for expanding the chart of nuclides and getting on the "island of stability." The possible number of bounded nuclides has been predicted to be around 9000, for which about 3340 have been observed up to now [1,2]. Most of radioactive nuclides are artificially made by radioactive ion beams (RIBs) facilities, and the undiscovered nuclides are mainly located on the neutron-rich regions.

To produce exotic neutron-rich isotopes, a series of experiments were carried out to produce heavy nuclei by multinucleon transfer (MNT) reactions [3–7]. Since the 1970s, plenty of new neutron-rich isotopes of elements from carbon to thorium were discovered in MNT reactions at JINR [8–11], Orsay [12,13], Berkeley [14–16], and GSI [17–21]. To observe the shell effects around $N = 126$, a series of experiments on ^{136}Xe + ^{208}Pb, ^{204}Hg + ^{198}Pt, and ^{136}Xe + ^{198}Pt have been performed at Argonne National Laboratory [22–27]. Watanabe *et al.* demonstrated the production cross sections of the $N = 126$ isotones in the ^{136}Xe + ^{198}Pt are extremely larger than those measured in the fragmentation reaction of a 1 GeV/nucleon ^{208}Pb beam impinged on a Be target [28]. At GANIL, the long-living components in the collision of ^{238}U + ^{238}U between 6.09 MeV/nucleon and 7.35 MeV/nucleon were investigated [29,30]. Thereafter, Kratz *et al.* have reexamined experimental data in the reactions of ^{238}U + ^{238}U and ^{238}U + ^{248}Cm at near-barrier energies, which showed that a considerable broadening of the fission-fragment mass distributions was observed [31].

Recently, deep-inelastic reactions involving ^{232}Th target nuclei at energies around the Coulomb barrier have been studied at Texas A&M [32–35]. In 2011, the reaction ^{197}Au + ^{232}Th at 7.50 MeV/nucleon has been studied using the BigSol spectrometer first. Large mass transfer is observed in the detected reaction products, giving rise to some nuclei with atomic numbers larger than 97 [32]. Further details of this experiment were presented in Majka *et al.* [33,34] along with plans to use an "active" catcher setup for further confirming $\Delta Z = +10$. In 2018, the production of α-particle decaying heavy nuclei in reactions of 6.10–7.50 MeV/nucleon ^{238}U + ^{232}Th was explored, which suggests that new activities with Z as high as 116 are being produced in this experiment [35]. However, the transuranic isotopic production cross sections in ^{197}Au + ^{232}Th and ^{238}U + ^{232}Th reactions are still unclear. One possible reason is that the cross sections of the superheavy nuclei are very low, the further information is required to make definitive atomic number and isotope identifications in the experiment. Thus, it is desirable to investigate the nucleon transfer limit and interaction mechanism of the reactions with ^{232}Th target on the production cross sections of exotic transuranic nuclei in theory.

*Corresponding author: fszhang@bnu.edu.cn

A lot of theoretical works have been devoted to study the MNT reaction mechanism in low-energy heavy-ion collisions. The semiclassical models such as the Grazing model [36,37], Grazing-F model [24], dinuclear system (DNS) model [38–49], and Langevin-type dynamical equations [50–53] have successfully described the production cross sections of heavy and superheavy nuclei. The microscopic dynamics models, such as the time-dependent Hartree-Fock (TDHF) model [54–60]and improved quantum molecular dynamics (ImQMD) model [61–65] have also shown reasonable success in describing the nucleon transport and energy dissipation in MNT reactions. Besides, an extension of the TDHF approach beyond the mean-field description has been proposed recently, which is referred to as the stochastic mean-field (SMF) approach [66–68]. In the DNS model, the transfer probability is calculated by solving a set of master equations numerically in the potential-energy surface [69,70]. The DNS model can describe the effects of quasi-elastic and deep-inelastic collisions, energy dissipation, N/Z equilibration, and shell structure in heavy-ion collisions. For more comprehensive reviews see Refs. [71–75].

The aim of this work is to produce unknown neutron-rich isotopes with $Z = 92$–106 by using the DNS model via ^{197}Au + ^{232}Th, ^{186}W + ^{232}Th, and ^{238}U + ^{232}Th reactions. The deexcitation process is treated with the GEMINI++ model.

This paper is organized as follows. In Sec. II, we describe the DNS model. The results and discussion are presented in Sec. III. Finally, we summarize the main results in Sec. IV.

II. THE MODEL

The dinuclear system (DNS) is formed at the initial stage of the reaction when the kinetic energy is transformed into the excitation energy of nuclei. Nucleon transfer occurs when the dinuclear system evolves to the minimum of the pocket of the nucleus-nucleus potential. For the heavy system without a potential pocket, the position where the nucleon transfer process takes place is R_{cont}, which is obtained with Eq. (3). The DNS model evolves as a diffusion process in the mass asymmetry degree of freedom $\eta = (A_1 - A_2)/A$ to the compound nucleus where A_1 and A_2 are the mass number of the nuclei and $A = A_1 + A_2$. In addition, a diffusion process in the variable R of the relative distance between the interacting nuclei occurs [76].

A. The potential-energy surface

In the DNS model, the potential-energy surface (PES) is crucial in the nucleon transfer process, which controls the evolution of a nuclear system in a multidimensional space. The driving potential is the PES under the minimum path. The PES is defined as [77]

$$U(Z_1, N_1, Z_2, N_2, R_{\rm cont}) = \Delta(Z_1, N_1) + \Delta(Z_2, N_2) + V_{\rm CN}(Z_1, N_1, Z_2, N_2, R_{\rm cont}, \theta_1, \theta_2), \quad (1)$$

where $\Delta(Z_i, N_i)(i = 1, 2)$ is mass excess of the two fragments. Z_i and N_i represent the number of protons and neutrons of the ith fragment, respectively. The mass excess of fragment (Z_i, N_i) can be written as

$$\Delta(Z, N) = Z\Delta_{\rm p} + N\Delta_{\rm n} - a_{\rm v}(1 - \kappa I^2)A + a_{\rm s}(1 - \kappa I^2)A^{2/3} + a_{\rm c}Z^2/A^{1/3} - c_4Z^2/A + E_{\rm pair}(Z_i, N_i) + E_{\rm shell}(Z_i, N_i). \quad (2)$$

Here, the liquid drop parameters are $a_{\rm v} = 15.677$ MeV, $a_{\rm s} = 18.560$ MeV, $a_{\rm c} = 0.717$ MeV, $\kappa = 1.790$, and $c_4 = 1.211$ MeV. $I = (N - Z)/A$ is the neutron-proton asymmetry of nucleus. The pairing energy $E_{\rm pair}(Z_i, N_i)$ and shell correction energy $E_{\rm shell}(Z_i, N_i)$ can be found in Ref. [78]. The position R_{cont}, where the nucleon transfer process takes place for a heavy reaction system, is given by the following formula:

$$R_{\rm cont} = R_1[1 + \beta_1 Y_{20}(\theta_1)] + R_2[1 + \beta_2 Y_{20}(\theta_2)] + 0.7\ {\rm fm}, \quad (3)$$

where $R_{1,2} = 1.16A_{1,2}^{1/3}$. β_1 and β_2 are the quadrupole deformation parameters of two fragments [78]. θ_1 and θ_2 are the angles between the collision axis and the symmetry axis of the deformed fragments. The interaction potential of the two fragments V_{CN} is expressed as

$$V_{\rm CN}(Z_1, N_1, Z_2, N_2, R, \beta_1, \beta_2) = V_{\rm C}(Z_1, N_1, Z_2, N_2, R, \beta_1, \beta_2) + V_{\rm N}(Z_1, N_1, Z_2, N_2, R, \beta_1, \beta_2), \quad (4)$$

where $V_{\rm C}$ and $V_{\rm N}$ are the Coulomb interaction potential [79] and the nuclear potential [77], respectively. The value of potential energy needed to overcome (ΔU) influence the nucleon transfer process. A smaller ΔU value generally results in a relatively high production cross section for the primary products. ΔU is defined as $\Delta U = U(Z_1, N_1, Z_2, N_2) - U(Z_P, N_P, Z_T, N_T)$. $U(Z_1, N_1, Z_2, N_2)$ and $U(Z_P, N_P, Z_T, N_T)$ are the PES corresponding to the configuration of $U(Z_1, N_1, Z_2, N_2)$ and the entrance point $U(Z_P, N_P, Z_T, N_T)$, respectively.

B. The master equation

The MNT processes between the interacting projectile and target are described as a diffusion process by solving a set of master equations in the corresponding PES. The time evolution of the probability distribution function $P(Z_1, N_1, E_1, t)$ for fragment 1 with Z_1, N_1, E_1 and time t is described by the master equations:

$$\frac{dP(Z_1, N_1, E_1, t)}{dt} = \sum_{Z_1'} W_{Z_1,N_1;Z_1',N_1}(t)[d_{Z_1,N_1}P(Z_1', N_1, E_1, t) - d_{Z_1',N_1}P(Z_1, N_1, E_1, t)] + \sum_{N_1'} W_{Z_1,N_1;Z_1,N_1'}(t)[d_{Z_1,N_1}P(Z_1, N_1', E_1, t) - d_{Z_1,N_1'}P(Z_1, N_1, E_1, t)]. \quad (5)$$

$W_{Z_1,N_1;Z_1',N_1}$ [or $W_{Z_1,N_1;Z_1,N_1'}$] is the mean transition probability from channel (Z_1, N_1) to (Z_1', N_1) [or from (Z_1, N_1) to

(Z_1, N_1')], which can be described as [80]

$$W_{Z_1,N_1;Z_1',N_1}(t) = \frac{\tau_{\rm mem}(Z_1, N_1, E_1; Z_1', N_1, E_1', t)}{d_{Z_1,N_1} d_{Z_1',N_1} \hbar^2} \times \sum_{ii'} |\langle Z_1', N_1, E_1', i'|V(t)|Z_1, N_1, E_1, i\rangle|^2. \tag{6}$$

Here, i represents the remaining quantum numbers. We assume that only one nucleon is transferred every step, namely $Z_1' = Z_1 \pm 1$ or $N_1' = N_1 \pm 1$. The memory time $\tau_{\rm mem}$ is expressed as

$$\tau_{\rm mem}(Z_1, N_1, E_1; Z_1', N_1, E_1'; t) = \hbar \left[\frac{2\pi}{\sum_{KK'} \langle V_{KK'} V_{KK'}^* \rangle} \right]^{1/2}, \tag{7}$$

and more details about $\tau_{\rm mem}$ can be found in Ref. [81].

The excitation energy of the DNS is defined as

$$E_{\rm DNS}^* = E_{\rm diss} - [U(Z_1, N_1, Z_2, N_2) - U(Z_P, N_P, Z_T, N_T)] - \frac{M^2}{2\zeta_{\rm int}}. \tag{8}$$

Here, M and $\zeta_{\rm int}$ denote the intrinsic angular momentum of the DNS and the intrinsic moment of inertia, respectively [82]. $E_{\rm diss}$ is the energy dissipating from the relative kinetic energy, which is given by

$$E_{\rm diss}(t) = E_{\rm c.m.} - V_{\rm CN}(Z_{\rm p}, N_{\rm p}, R_{\rm cont}) - \frac{\langle J(t)\rangle^2}{2\zeta_{\rm rel}} - E_{\rm rad}(t), \tag{9}$$

where $V_{\rm CN}(Z_{\rm p}, N_{\rm p}, R_{\rm cont})$ is the interaction potential corresponding to the entrance channel. The dissipation of the relative angular momentum $\langle J(t)\rangle$, which can be calculated by $\langle J(t)\rangle = J_{st} + (J - J_{st})\exp[-t/\tau_J)]$. J_{st} is the angular momentum at the sticking limit. The radial energy at time t is given by $E_{\rm rad}(t) = E_{\rm rad}(t=0)\exp(-t/\tau_{\rm R})$, where $\tau_{\rm R}$ is the relaxation time of the radial kinetic energy.

C. Deexcitation process

In the DNS model, the production cross sections of the primary products with proton number Z_1 and neutron number N_1 in transfer processes are calculated by the following expression:

$$\sigma_{\rm pr}(Z_1, N_1, E_{\rm c.m.}) = \frac{\pi\hbar^2}{2\mu E_{\rm c.m.}} \sum_J (2J+1) \times [P(Z_1, N_1, E_1, t = \tau_{\rm int})]. \tag{10}$$

Here, μ is the reduced mass of the system and $E_{\rm c.m.}$ is the incident energy in the center-of-mass frame. P is the fragment distribution probability and $\tau_{\rm int}$ is the interaction time [83].

The statistical model GEMINI++ is used to deal with the subsequent deexcited process of excited fragments [84,85]. The GEMINI++ code takes into account evaporation of light charged particles, symmetric fission, and all possible evaporation channels. Furthermore, the Hauser-Feshbach theory was used in this code for the evaporation of light particles. For the emission of heavier fragments and asymmetric fission of a heavy system, the GEMINI++ model not only adopts Moretto formalism theory, but also considers the structure evolution based on the Bohr-Wheeler formalism.

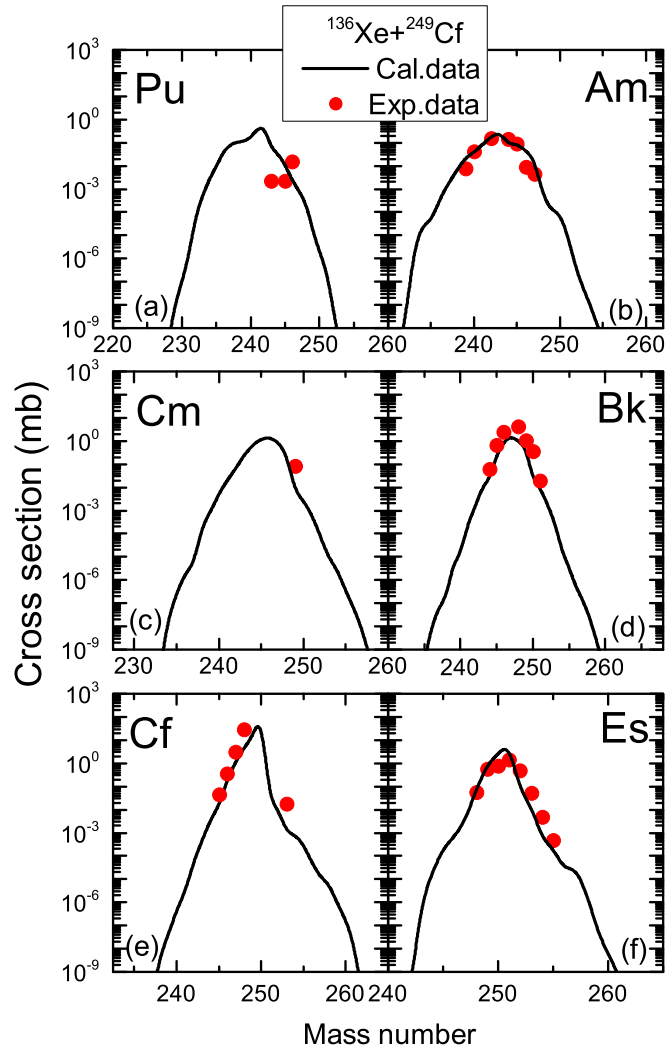

FIG. 1. The final isotopic production cross sections of (a) Pu, (b) Am, (c) Cm, (d) Bk, (e) Cf, and (f) Es in the ^{136}Xe + ^{249}Cf reaction (black solid lines). The incident energy is $E_{\rm c.m.} = 567$ MeV. The red solid circles represent the experimental data, which are taken from the Ref. [86].

III. RESULTS AND DISCUSSION

A. Comparison with experimental data

Motivated by testing the reliability of using the DNS model to predict the production of transuranium isotopes, we present the production cross sections of nuclei with $Z = 94$–99 in the reaction ^{136}Xe + ^{249}Cf at $E_{\rm c.m.} = 567$ MeV in Fig. 1. The black solid lines represent the calculation results of Pu, Am, Cm, Bk, Cf, and Es in Figs. 1(a)–1(f), respectively. The experimental data were obtained from the Ref. [86]. From Fig. 1, one can see that the calculated results are in good agreement

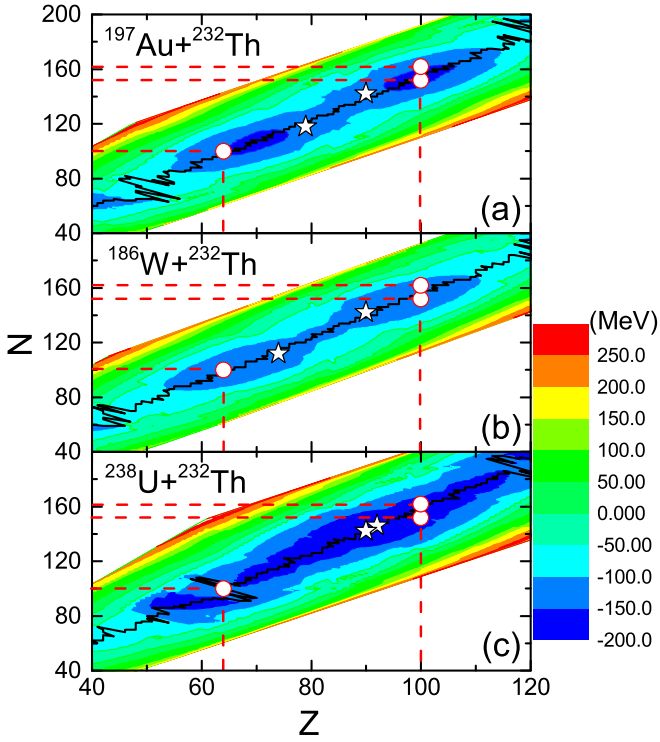

FIG. 2. The potential-energy surface (PES) as a function of Z and N of the fragments in the reactions of (a) $^{197}\mathrm{Au}+^{232}\mathrm{Th}$, (b) $^{186}\mathrm{W}+^{232}\mathrm{Th}$, and (c) $^{238}\mathrm{U}+^{232}\mathrm{Th}$. The black solid lines indicate the minimum value in the PES. The open stars and circles represent the injection points and the positions of subshell, respectively.

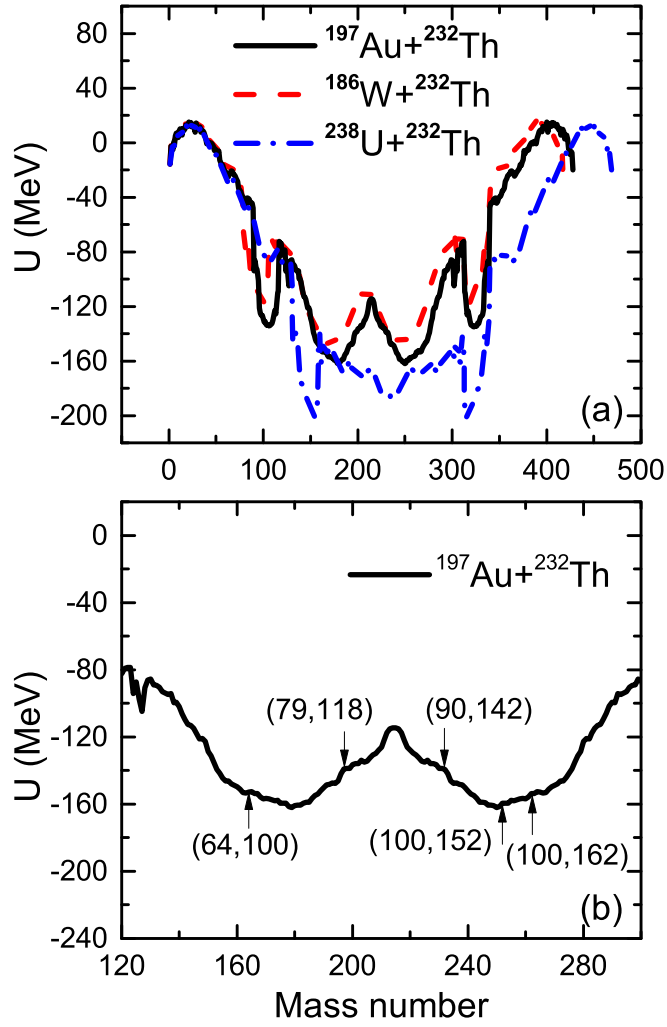

FIG. 3. (a) The driving potentials in collisions of $^{197}\mathrm{Au}+^{232}\mathrm{Th}$ (black solid line), $^{186}\mathrm{W}+^{232}\mathrm{Th}$ (red dashed line), and $^{238}\mathrm{U}+^{232}\mathrm{Th}$ (blue dash-dotted line). (b) The driving potential in the reaction of $^{197}\mathrm{Au}+^{232}\mathrm{Th}$. The upward and downward arrows indicate the positions of subshell and the incident channels, respectively.

with the measured data. The peak position of the theoretical calculated section is near to the experimental one. The decreasing of calculated isotopic distribution cross sections is not obvious with increasing proton number of the target-like fragments (TLFs). For instance, the peak value of the production cross section for Es [see Fig. 1(f)] is still within one order of magnitude compared with the peak value of Pu [see Fig. 1(a)]. While the projectile of the $^{136}\mathrm{Xe}+^{249}\mathrm{Cf}$ system is lighter than those of the reaction systems studied in this paper, the nuclides investigated in these reactions are all distributed in the transuranic region. Therefore, it is reasonable to apply the DNS model plus GEMINI++ code to predict the production of transuranium isotopes.

B. The "inverse" quasifission process in the $^{197}\mathrm{Au}+^{232}\mathrm{Th}$ reaction

For producing the neutron-rich transuranium nuclei with $Z = 92$–106, the "inverse" quasifission process is vital, which leads to nucleons mainly transfer from the light partner to the heavy one [46]. To search for the optimal projectile-target combination, we investigate the MNT process induced by $^{197}\mathrm{Au}$, $^{186}\mathrm{W}$, and $^{238}\mathrm{U}$ beams with actinide target $^{232}\mathrm{Th}$ in this work. The shape of the three-dimensional PES plays an essential role in the calculation of fragments formation probabilities in the transfer process. In Fig. 2, we show the PES as a function of Z and N of the fragments in the reactions of $^{197}\mathrm{Au}+^{232}\mathrm{Th}$, $^{186}\mathrm{W}+^{232}\mathrm{Th}$, and $^{238}\mathrm{U}+^{232}\mathrm{Th}$, respectively. Here, the black solid lines indicate the minimum value in the PES. The open stars and circles represent the injection points and the positions of the subshell, respectively.

From Fig. 2(a) and Fig. 2(b), it is clear that $^{197}\mathrm{Au}+^{232}\mathrm{Th}$ and $^{186}\mathrm{W}+^{232}\mathrm{Th}$ reaction systems are the "inverse" quasifission process, whose PES show two valleys away from the injection points. This may be due to the subshell closures near $Z = 64$, 100 and $N = 100$, 152, 162, which will be discussed in detail in Fig. 3(b). The subshell effects on the PES around the injection point are more obvious than those in the reaction $^{197}\mathrm{Au}+^{232}\mathrm{Th}$, which could strongly influence the nucleon transfer at low incident energies. Furthermore, it can be seen that the PES of injection point $^{197}\mathrm{Au}$ in Fig. 2(a) is not located at the valley, which is higher than that valley. This means that the nucleon transfer process moves in the direction of increasing mass asymmetry of reaction system. In contrast, for the reaction $^{238}\mathrm{U}+^{232}\mathrm{Th}$ in Fig. 2(c), the

incident channel is in the minimum valley, which indicate that this reaction transfer process is a general quasifission process.

Motivated by investigating the process of nucleon transfer direction in the "inverse" quasifission process more deeply, the driving potential as a function of the mass number of fragments in collisions of ^{197}Au + ^{232}Th, ^{186}W + ^{232}Th, and ^{238}U + ^{232}Th are shown in Fig. 3. The upward and downward arrows indicate the positions of subshell and the positions of entrance channels, respectively. Compared with the other two reaction systems in Fig. 3(a), the driving potential of ^{186}W + ^{232}Th is rather high. For the reactions of ^{186}W + ^{232}Th and ^{197}Au + ^{232}Th, the nucleon transfer process is supposed to increase the mass asymmetry of the outgoing fragments. Moreover, it can be clearly seen that one deep valley appears around the configuration of ^{238}U + ^{232}Th. As mentioned above, the transfer process in the collision of ^{238}U + ^{232}Th is a standard quasifission process. The N/Z ratio of ^{238}U is 1.58, which is slightly larger than 1.57 ratio of the target ^{232}Th. Due to the N/Z ratio equilibrium, there is a trend to transfer neutrons from projectile ^{238}U to the target ^{232}Th. In Fig. 3(b), due to the subshell effects near $Z = 64, 100$ and $N = 100, 152, 162$, there are two deep pockets in the driving potential corresponding to the ^{197}Au + ^{232}Th reaction. This means that it is easier for the projectile nucleus to transfer nucleons to target under the driving force. This is consistent with the conclusions for the ^{156,160}Gd + ^{186}W reactions in Refs. [87,88].

To clarify the transfer process more clearly in three systems, we extract the values of ΔU in Fig. 4. Figures 4(a) and 4(b) represent the pure neutron stripping channel and pure proton stripping channel, respectively. From Fig. 4(a), one can find that the ΔU values decrease and then increase with the increasing number of neutron stripping. Meanwhile, compared with other reaction systems, the lowest potential need to overcome in the ^{197}Au + ^{232}Th reaction in the larger neutron stripping channel. For example, in the case of stripping six neutrons, the values of ΔU in the reactions of ^{197}Au + ^{232}Th, ^{186}W + ^{232}Th, and ^{238}U + ^{232}Th are 3.693, 12.243, and 7.110 MeV, respectively. This means that the pure neutron stripping in the ^{197}Au + ^{232}Th reaction is easier than that in ^{186}W + ^{232}Th and ^{238}U + ^{232}Th reactions.

In Fig. 4(b), it can be noticed that with an increasing number of stripping protons, the ΔU values decrease first and then increase. For the ^{186}W + ^{232}Th and ^{238}U + ^{232}Th reactions, the ΔU values in pure proton stripping show an opposite behavior to the ΔU values in pure neutron stripping. This indicates that the proton stripping for ^{186}W + ^{232}Th is easier compared with the ^{238}U + ^{232}Th reaction, while the neutron stripping is opposite in Fig. 4(a). The ΔU values are the lowest in the ^{197}Au + ^{232}Th reaction when one to six protons are stripped from the projectile. For instance, in the case of stripping six protons, the values of ΔU in the reactions of ^{197}Au + ^{232}Th, ^{186}W + ^{232}Th, and ^{238}U + ^{232}Th are −4.029, 6.997, and 13.203 MeV, respectively. To produce new neutron-rich transuranium isotopes, it is expected that the target obtain protons and neutrons in the transfer process. Thus, ^{197}Au + ^{232}Th is a favorable candidate for the experimental research.

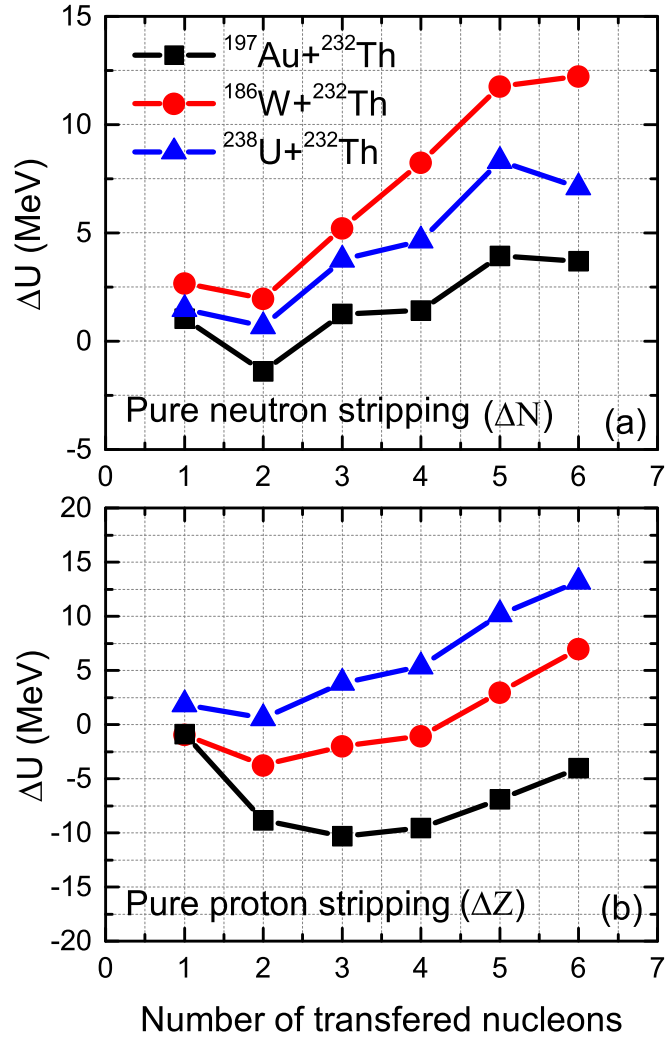

FIG. 4. The ΔU values in the (a) pure neutron stripping and (b) pure proton stripping channels in the transfer reactions ^{197}Au + ^{232}Th (square symbols), ^{186}W + ^{232}Th (circle symbols), and ^{238}U + ^{232}Th (triangle symbols).

C. The entrance channel and incident energy effects on the yields of target-like fragments

In some earlier experiments, Wuenchel *et al.* used the BigSol Spectrometer at Texas A&M to perform several surveys of projectile-target combinations and bombarding energy for the collision of ^{197}Au with ^{232}Th in an effort to identify good candidate reactions for heavy and superheavy element production [32–34]. However, these experiments only indicate the possible production of heavy elements with Z above 97, and the new neutron-rich isotopic distribution cross sections are not yet given clearly.

To find the optimal two colliding partners, the production cross sections of new neutron-rich isotopes in the ^{197}Au + ^{232}Th (black solid lines), ^{186}W + ^{232}Th (red dashed lines), and ^{238}U + ^{232}Th (blue dash-dotted lines) transfer reactions at $E_{\mathrm{c.m.}} = 1.10V_B$ are presented in Fig. 5. Here, V_B is the Bass interaction barrier [89]. The V_B values for the ^{197}Au + ^{232}Th, ^{186}W + ^{232}Th, and ^{238}U + ^{232}Th reactions are

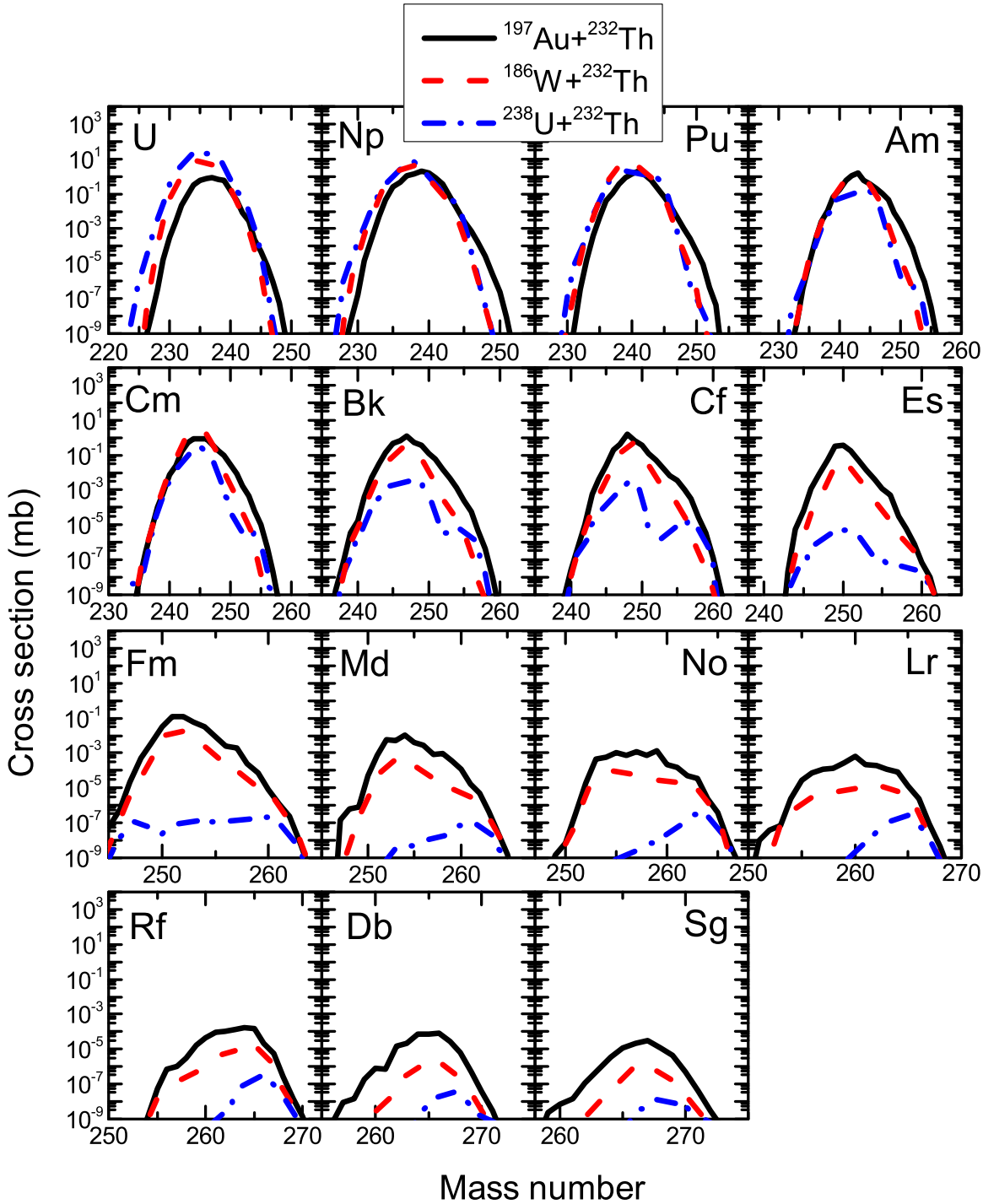

FIG. 5. The final isotopic production cross sections of TLFs with $Z = 92$–106 in the transfer reactions $^{197}\mathrm{Au} + {}^{232}\mathrm{Th}$ (black solid lines), $^{186}\mathrm{W} + {}^{232}\mathrm{Th}$ (red dashed lines), and $^{238}\mathrm{U} + {}^{232}\mathrm{Th}$ (blue dash-dotted lines) at $E_{\mathrm{c.m.}} = 1.10V_B$, respectively. V_B is the Bass interaction barrier.

657.8, 619.3, and 748.9 MeV, respectively. One can see that the production cross sections on the neutron-rich side for the $^{197}\mathrm{Au} + {}^{232}\mathrm{Th}$ reaction are largest. This is mainly due to the smallest ΔU values along the pure neutron stripping and pure proton stripping channels, as shown in the Figs. 4(a) and 4(b), respectively.

From Fig. 5, it also can be found that the production cross sections for the most final transuranium fragments decrease almost exponentially with the increase of the fragment charge number, especially in the reaction of $^{238}\mathrm{U} + {}^{232}\mathrm{Th}$. One important reason is that the fission barrier heights for light uranium-like nuclei are much higher than those for heavy transuranium nuclei so that most of light primary uranium-like fragments survive fission and heavy transuranium nuclei hardly survive fission. Hence, we consider $^{197}\mathrm{Au} + {}^{232}\mathrm{Th}$ is a favorable candidate to

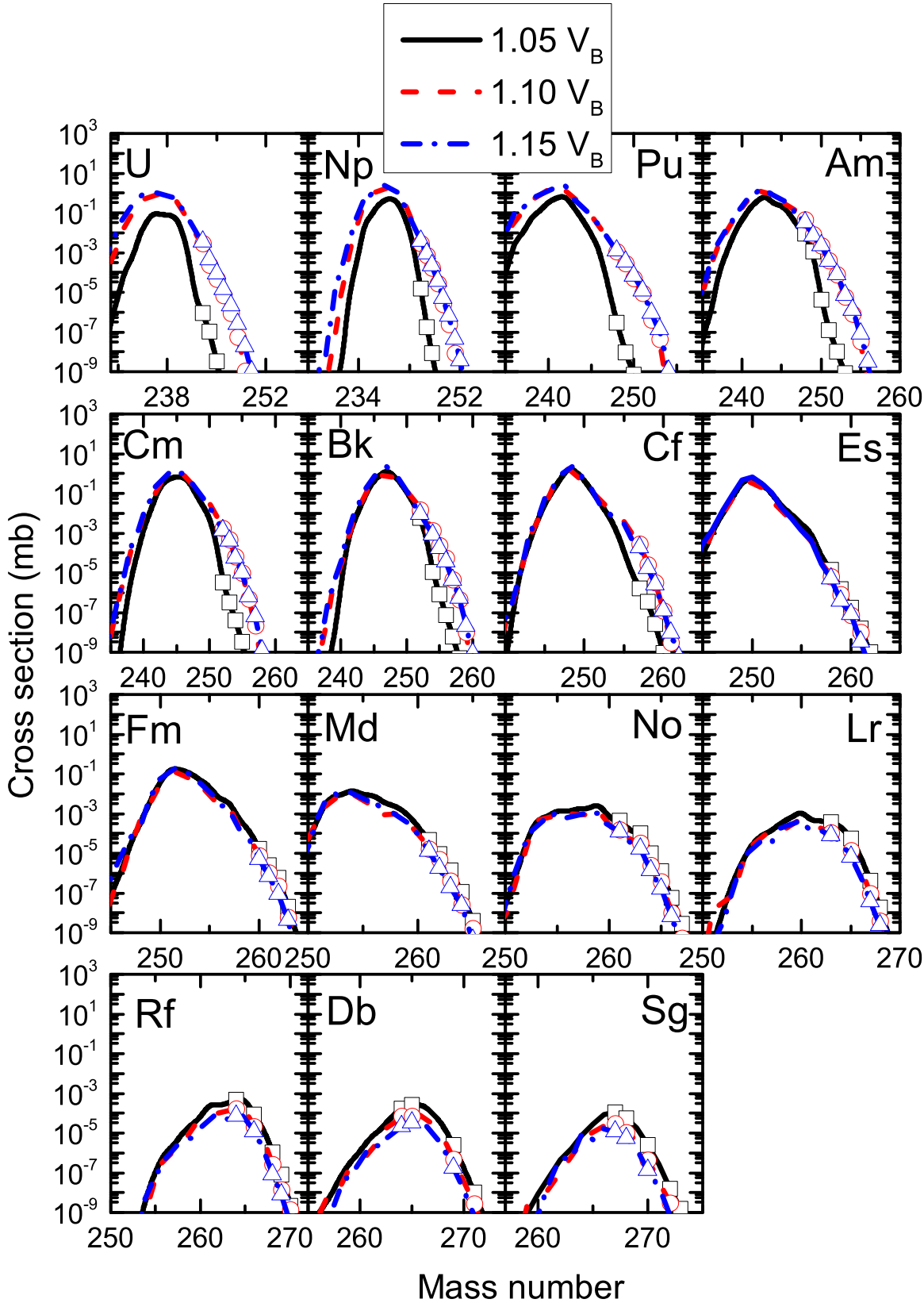

FIG. 6. The final isotopic production cross sections of TLFs with $Z = 92$–106 in the transfer reaction $^{197}\mathrm{Au} + ^{232}\mathrm{Th}$ at $E_{\mathrm{c.m.}} = 1.05V_B$ (black solid lines), $1.10V_B$ (red dashed lines), and $1.15V_B$ (blue dash-dotted lines), respectively. The blank square, circle, and triangle symbols denote the unknown neutron-rich nuclei produced at $E_{\mathrm{c.m.}} = 1.05V_B$, $1.10V_B$, and $1.15V_B$, respectively.

produce new neutron-rich isotopes with $Z = 92$–106 in MNT reaction.

The $^{197}\mathrm{Au} + ^{232}\mathrm{Th}$ reaction gives a significant advantage when producing new neutron-rich isotopes with $Z = 92$–106 due to the "inverse" quasifission process as discussed above. For further investigating the optimal energy, the final isotopic production cross sections of TLFs in the transfer reaction $^{197}\mathrm{Au} + ^{232}\mathrm{Th}$ at different incident energies are shown in Fig. 6. The black solid lines, red dashed lines, and blue dashed-dotted lines represent the $E_{\mathrm{c.m.}} = 1.05V_B$, $1.10V_B$, and $1.15V_B$, respectively. The blank square, triangle, and circle symbols denote the unknown neutron-rich nuclei produced at $E_{\mathrm{c.m.}} = 1.05V_B$, $1.10V_B$, and $1.15V_B$, respectively.

In Fig. 6, it can be easily found that the final production cross sections decrease by four orders of the magnitude from U to Sg and the peak locations shift to the heavier mass side with more protons transferred. Besides, a weaker energy dependence is observed at $E_{\mathrm{c.m.}} = 1.05V_B$–$1.15V_B$ on the neutron-deficient side. While in the case of the neutron-rich side, the dependence of production cross-section distributions for TLFs from U to Cf on incident energy becomes stronger with the charge number increases. It is found that the production cross sections of neutron-rich isotopes at $1.15V_B$ are larger than those at $1.05V_B$ and $1.10V_B$. The final cross sections from Es to Sg on the neutron-rich side are almost the same at different incident energies with the increase of charge number. This is attributed to a larger incident energy can increase the transfer probability of nucleons, which leads to an increase in the primary cross section on the neutron-rich side. However, as the excitation energy further increased, the fission probability becomes larger, resulting in the survival probability of these heavy nuclei lower. Although the final production cross sections from Es to Sg on the neutron-rich side at such energies are fairly close, it can be seen that the production cross sections appear maximum at $E_{\mathrm{c.m.}} = 1.05V_B$. For example, five new neutron-rich nuclei $^{267,268,270,272,273}\mathrm{Sg}$ at $1.05V_B$ are predicted. While in the case of $1.15V_B$, only predicted three unknown nuclei $^{267,268,270}\mathrm{Sg}$. Overall, the $E_{\mathrm{c.m.}} = 1.15V_B$ is more suitable for producing new neutron-rich isotopes with $Z = 92$–98, and $E_{\mathrm{c.m.}} = 1.05V_B$ is the optimal incident energy for the production of neutron-rich transuranium isotopes with $Z = 99$–106 in the $^{197}\mathrm{Au} + ^{232}\mathrm{Th}$ reaction.

The influence of the incident energy on interaction time in reaction $^{197}\mathrm{Au} + ^{232}\mathrm{Th}$ is also investigated. Figure 7 depicts the calculated interaction time as a function of the impact parameter for the system of $^{197}\mathrm{Au} + ^{232}\mathrm{Th}$ at four different incident energies. The solid, dashed, dotted, and dash-dotted lines indicate the incident energy at $E_{\mathrm{c.m.}} = 1.05V_B$, $1.10V_B$, $1.15V_B$, and $1.20V_B$, respectively. Here, the reaction time is calculated by deflection function [90]. From Fig. 7, it is noticed that the interaction time decrease with the increasing of impact parameters. Meanwhile, the range of impact parameters and interaction time increase with the increase of incident energy. This is because with the incident energy increases, the internal excitation energy dissipated in the dinuclear system increases, leading to the interaction distance and evolution time between the two nuclei increase.

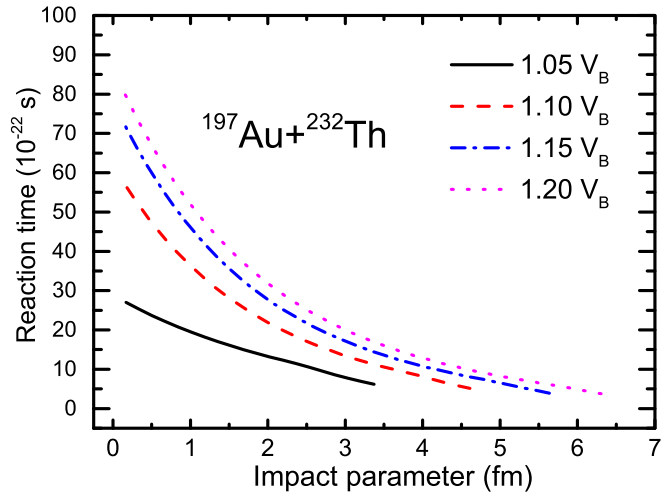

FIG. 7. The calculated interaction time as a function of the impact parameter for the system of $^{197}\mathrm{Au} + ^{232}\mathrm{Th}$ at four different incident energies. The solid, dashed, dash-dotted, and dotted lines indicate the incident energy at $E_{\mathrm{c.m.}} = 1.05V_B$, $1.10V_B$, $1.15V_B$, and $1.20V_B$, respectively.

D. Production cross sections of unknown neutron-rich transuranium nuclei

According to the discussion in the last section, the reaction $^{197}\mathrm{Au} + ^{232}\mathrm{Th}$ is an optimal combination for producing neutron-rich transuranium isotopes with $Z = 92$–106. Moreover, the $E_{\mathrm{c.m.}} = 1.15V_B$ is more suitable for producing the new neutron-rich isotopes with $Z = 92$–98. While $E_{\mathrm{c.m.}} = 1.05V_B$ is the optimal incident energy for the production of neutron-rich transuranium isotopes with $Z = 99$–106.

The predicted cross sections of unknown isotopes with $Z = 92$–106 via $^{197}\mathrm{Au} + ^{232}\mathrm{Th}$ reaction at corresponding incident energies with DNS model are given in Table I. It is found that 88 unknown exotic neutron-rich isotopes of U, Np, Pu, Am, Cm, Bk, Cf, Es, Fm, Md, No, Lr, Rf, Db, and Sg would expect to be produced with cross sections greater than 1 pb. From Table I, it is obvious that the yield becomes lower with more neutrons transferred at the same incident energy due to larger ΔU values. For instance, at the same energy $E_{\mathrm{c.m.}} = 1.15V_B$ (756.47 MeV), the production cross sections of $^{249}\mathrm{U}$ (1.87×10^{-5} μb) is much smaller than $^{243}\mathrm{U}$ (3.35 μb), while ΔU value of $^{249}\mathrm{U}$ (17.07 MeV) is rather large than $^{243}\mathrm{U}$ (-3.26 MeV). Also, it is noticed that the ΔU values of all predicted new nuclides, both positive and negative, are less than 20 MeV. This means that the nucleon transfer in the $^{197}\mathrm{Au} + ^{232}\mathrm{Th}$ reaction would be easier. In these TLFs of Table I, we can also predict that the upper limit for the production of the heaviest new nuclide is $^{273}\mathrm{Sg}$. It indicates that 16 protons and 25 neutrons are transferred from the projectile $^{197}\mathrm{Au}$ to the target $^{232}\mathrm{Th}$ for producing the final fragment $^{273}\mathrm{Sg}$.

IV. CONCLUSIONS

The reaction $^{197}\mathrm{Au} + ^{232}\mathrm{Th}$ was investigated at Texas A&M using the BigSol as a velocity spectrometer for

TABLE I. The production cross sections of predicted unknown isotopes with $Z = 92$–106 in the $^{197}\mathrm{Au} + ^{232}\mathrm{Th}$ transfer reaction at $1.15V_B$ and $1.05V_B$.

Isotope	$E_{\mathrm{c.m.}}/V_B$	ΔU	σ_{cal} (μb)
^{243}U	1.15	−3.26	3.35
^{244}U	1.15	−3.02	0.43
^{245}U	1.15	−0.99	8.66×10^{-2}
^{246}U	1.15	3.08	1.37×10^{-2}
^{247}U	1.15	8.07	2.11×10^{-3}
^{248}U	1.15	12.84	2.38×10^{-4}
^{249}U	1.15	17.07	1.87×10^{-5}
^{245}Np	1.15	−9.41	3.90
^{246}Np	1.15	−6.00	0.90
^{247}Np	1.15	−2.38	0.22
^{248}Np	1.15	1.98	3.66×10^{-2}
^{249}Np	1.15	6.77	5.05×10^{-3}
^{250}Np	1.15	10.59	6.38×10^{-4}
^{251}Np	1.15	14.60	4.56×10^{-5}
^{252}Np	1.15	19.69	3.71×10^{-6}
^{248}Pu	1.15	−6.77	1.20
^{249}Pu	1.15	−2.92	0.34
^{250}Pu	1.15	1.46	6.40×10^{-2}
^{251}Pu	1.15	5.76	1.20×10^{-2}
^{252}Pu	1.15	9.43	9.07×10^{-4}
^{253}Pu	1.15	13.90	1.36×10^{-4}
^{254}Pu	1.15	17.96	1.13×10^{-6}
^{248}Am	1.15	−14.81	32.87
^{249}Am	1.15	−12.15	6.96
^{250}Am	1.15	−8.87	2.18
^{251}Am	1.15	−5.81	0.36
^{252}Am	1.15	−2.06	7.62×10^{-2}
^{253}Am	1.15	1.20	6.90×10^{-3}
^{254}Am	1.15	4.40	1.30×10^{-3}
^{255}Am	1.15	8.95	8.00×10^{-5}
^{256}Am	1.15	14.47	3.02×10^{-6}
^{252}Cm	1.15	−11.70	1.36
^{253}Cm	1.15	−6.40	0.39
^{254}Cm	1.15	−4.44	5.72×10^{-2}
^{255}Cm	1.15	−0.82	9.88×10^{-3}
^{256}Cm	1.15	2.41	6.58×10^{-4}
^{257}Cm	1.15	7.56	6.34×10^{-5}
^{258}Cm	1.15	12.31	1.17×10^{-6}
^{252}Bk	1.15	−15.72	8.94
^{254}Bk	1.15	−10.85	0.84
^{255}Bk	1.15	−9.39	0.17
^{256}Bk	1.15	−6.30	3.53×10^{-2}
^{257}Bk	1.15	−3.41	4.17×10^{-3}
^{258}Bk	1.15	1.24	5.30×10^{-4}
^{259}Bk	1.15	4.61	1.95×10^{-5}
^{257}Cf	1.15	−9.39	0.19
^{258}Cf	1.15	−7.53	1.69×10^{-2}
^{259}Cf	1.15	−4.16	2.50×10^{-3}
^{260}Cf	1.15	−1.35	1.21×10^{-4}
^{261}Cf	1.15	4.79	9.34×10^{-6}
^{258}Es	1.05	−12.86	1.47×10^{-2}
^{259}Es	1.05	−11.99	1.45×10^{-3}
^{260}Es	1.05	−8.08	1.79×10^{-4}
^{261}Es	1.05	−5.60	1.57×10^{-5}
^{262}Es	1.05	0.03	1.03×10^{-6}
^{260}Fm	1.05	−14.25	1.68×10^{-2}
^{261}Fm	1.05	−10.90	2.58×10^{-3}
^{262}Fm	1.05	−8.95	5.80×10^{-4}
^{263}Fm	1.05	−4.67	1.99×10^{-5}
^{261}Md	1.05	−15.86	4.57×10^{-2}
^{262}Md	1.05	−13.06	9.44×10^{-3}
^{263}Md	1.05	−11.57	1.36×10^{-3}
^{264}Md	1.05	−7.77	1.10×10^{-4}
^{265}Md	1.05	−5.38	4.13×10^{-6}
^{261}No	1.05	−16.63	0.43
^{263}No	1.05	−14.05	0.10
^{264}No	1.05	−14.06	9.61×10^{-3}
^{265}No	1.05	−9.90	1.21×10^{-3}
^{266}No	1.05	−8.79	5.79×10^{-5}
^{267}No	1.05	−2.63	2.79×10^{-6}
^{263}Lr	1.05	−16.38	0.36
^{265}Lr	1.05	−15.21	5.37×10^{-2}
^{267}Lr	1.05	−10.88	4.02×10^{-3}
^{268}Lr	1.05	−5.28	1.86×10^{-5}
^{264}Rf	1.05	−15.08	0.49
^{266}Rf	1.05	−16.10	8.94×10^{-2}
^{268}Rf	1.05	−11.83	1.07×10^{-4}
^{269}Rf	1.05	−6.72	7.73×10^{-4}
^{270}Rf	1.05	−4.81	2.10×10^{-6}
^{264}Db	1.05	−13.42	0.17
^{265}Db	1.05	−15.56	0.27
^{269}Db	1.05	−12.34	2.60×10^{-3}
^{271}Db	1.05	−6.42	1.02×10^{-5}
^{267}Sg	1.05	−12.48	0.11
^{268}Sg	1.05	−13.77	5.57×10^{-2}
^{270}Sg	1.05	−11.53	2.47×10^{-3}
^{272}Sg	1.05	−6.48	1.54×10^{-5}
^{273}Sg	1.05	−1.69	1.57×10^{-6}

superheavy elements production. A large mass transfer is observed in the detected reaction products with Z above 97, but a precise identification of these nuclei, such as isotopic cross section, has not been given yet [32–34]. Thus, the corresponding theoretical calculations are expected to be able to describe the transfer limit and dynamical mechanisms in the reactions with ^{232}Th target.

The synthesis of neutron-rich isotopes in the range of $Z = 92$–106 is studied in MNT reactions based on the DNS model with GEMINI++ code. This work compares the calculation results with the experimental data of the reaction $^{136}\mathrm{Xe} + ^{249}\mathrm{Cf}$ at $E_{\mathrm{c.m.}} = 567$ MeV, and the results show that the DNS model with GEMINI++ code is suitable to describe the MNT reactions of the heavy-mass systems.

To produce the exotic neutron-rich transuranium nuclei, the MNT reactions of $^{186}\mathrm{W} + ^{232}\mathrm{Th}$, $^{197}\mathrm{Au} + ^{232}\mathrm{Th}$, and $^{238}\mathrm{U} + ^{232}\mathrm{Th}$ are investigated. Due to subshell effects of $Z = 64, 100$ and $N = 100, 152, 162$, the "inverse" quasifission process is found in the collisions of $^{186}\mathrm{W} + ^{232}\mathrm{Th}$ and $^{197}\mathrm{Au} + ^{232}\mathrm{Th}$, which enhances the cross sections of neutron-rich transuranium nuclei. Along the pure neutron stripping and proton stripping channels, the ΔU values

in the transfer reactions ^{197}Au + ^{232}Th are smallest. The production cross sections of neutron-rich nuclei in the reaction ^{197}Au + ^{232}Th are larger than that in ^{186}W + ^{232}Th and ^{238}U + ^{232}Th. Hence, ^{197}Au + ^{232}Th is a promising candidate for producing neutron-rich nuclei.

The effect of the incident energy on the yields of TLFs in the ^{197}Au + ^{232}Th reaction is also studied. For producing neutron-rich isotopes with $Z = 92$–98, $E_{\text{c.m.}} = 756.47$ MeV is more suitable. While for the production of TLFs with $Z = 99$–106, $E_{\text{c.m.}} = 690.69$ MeV is the optimal incident energy. The effect of energy on the interaction time is investigated. The interaction time increases with the increase of energy in the interval from $E_{\text{c.m.}} = 1.05V_B$ to $E_{\text{c.m.}} = 1.20V_B$. We predict that 88 unknown heavy neutron-rich nuclei around $Z = 92 - 106$ can be produced with cross sections at the order of 10^{-6} to 10 μb. This also confirms the possibility of producing nuclei with Z above 97 in the collision of ^{197}Au + ^{232}Th in Ref. [32].

ACKNOWLEDGMENTS

This work was supported by the National Natural Science Foundation of China under Grants No. 12135004, No. 11635003, No. 11961141004, No. 12105019, and No. 12047513; the Beijing Postdoctoral Research Foundation (2021-zz-089); and the Guangxi Science and Technology Base and Special Talent Program under Grant No. 2021AC19266.

[1] M. Thoennessen, *The Discovery of Isotopes: A Complete Compilation* (Springer International Publishing, New York, 2016), pp. 1–384.
[2] https://people.nscl.msu.edu/~thoennes/isotopes/ (2022).
[3] G. Seaborg, W. Loveland, and D. Morrissey, Science **203**, 711 (1979).
[4] W. Loveland, Front. Phys. **7**, 23 (2019).
[5] S. Heinz and H. Devaraja, Eur. Phys. J. A **58**, 114 (2022).
[6] L. Corradi, G. Pollarolo, and S. Szilner, J. Phys. G **36**, 113101 (2009).
[7] F. S. Zhang, C. Li, L. Zhu, and P. W. Wen, Front. Phys. **13**, 132113 (2018).
[8] A. Artukh, G. Gridnev, V. Mikheev, and V. Volkov, Nucl. Phys. A **137**, 348 (1969).
[9] G. Gridnev, V. Volkov, and J. Wilczynski, Nucl. Phys. A **142**, 385 (1970).
[10] A. Artukh, V. Avdeichikov, G. Gridnev, V. Mikheev, V. Volkov, and J. Wilczynski, J. Phys., Colloq. **32**, C6 (1971).
[11] A. Artukh, G. Gridnev, V. Mikheev, V. Volkov, and J. Wilczynski, Nucl. Phys. A **211**, 299 (1973).
[12] J. Galin, D. Guerreau, M. Lefort, J. Peter, X. Tarrago, and R. Basile, Nucl. Phys. A **159**, 461 (1970).
[13] F. Hanappe, M. Lefort, C. Ngô, J. Péter, and B. Tamain, Phys. Rev. Lett. **32**, 738 (1974).
[14] J. V. Kratz, A. E. Norris, and G. T. Seaborg, Phys. Rev. Lett. **33**, 502 (1974).
[15] J. V. Kartz, J. O. Liljenzin, A. E. Norris, and G. T. Seaborg, Phys. Rev. C **13**, 2347 (1976).
[16] R. J. Otto, M. M. Fowler, D. Lee, and G. T. Seaborg, Phys. Rev. Lett. **36**, 135 (1976).
[17] K. L. Gippert, E. Runte, W. D. Schmidt-Ott, P. Tidemand-Petersson, N. Kaffrell, P. Peuser, R. Kirchner, O. Klepper, W. Kurcewicz, P. Larsson, E. Roeckl, D. Schardt, and K. Rykaczewski, Nucl. Phys. A **453**, 1 (1986).
[18] K. D. Hildenbrand, H. Freiesleben, F. Pühlhofer, W. F. W. Schneider, R. Bock, D. v. Harrach, and H. J. Specht, Phys. Rev. Lett. **39**, 1065 (1977).
[19] M. Schädel, J. V. Kratz, H. Ahrens, W. Brüchle, G. Franz, H. Gäggeler, I. Warnecke, G. Wirth, G. Herrmann, N. Trautmann, and M. Weis, Phys. Rev. Lett. **41**, 469 (1978).
[20] M. Schädel, W. Brüchle, H. Gäggeler, J. V. Kratz, K. Sümmerer, G. Wirth, G. Herrmann, R. Stakemann, G. Tittel, N. Trautmann, J. M. Nitschke, E. K. Hulet, R. W. Lougheed, R. L. Hahn, and R. L. Ferguson, Phys. Rev. Lett. **48**, 852 (1982).
[21] M. Götz, S. Götz, J. Kratz, C. Düllmann, C. Mokry, J. Runke, P. Thörle-Pospiech, N. Wiehl, M. Schädel, J. Ballof, H. Dorrer, J. Grund, D. Huber, E. Jäger, O. Keller, J. Krier, J. Khuyagbaatar, L. Lens, B. Lommel, M. Mendel *et al.*, Nucl. Phys. A **961**, 1 (2017).
[22] J. V. Kratz, W. Loveland, and K. J. Moody, Nucl. Phys. A **944**, 117 (2015).
[23] J. S. Barrett, W. Loveland, R. Yanez, S. Zhu, A. D. Ayangeakaa, M. P. Carpenter, J. P. Greene, R. V. F. Janssens, T. Lauritsen, E. A. McCutchan, A. A. Sonzogni, C. J. Chiara, J. L. Harker, and W. B. Walters, Phys. Rev. C **91**, 064615 (2015).
[24] R. Yanez and W. Loveland, Phys. Rev. C **91**, 044608 (2015).
[25] T. Welsh, W. Loveland, R. Yanez, J. S. Barrett, E. A. McCutchan, A. A. Sonzogni, T. Johnson, S. Zhu, J. P. Greene, A. D. Ayangeakaa, M. P. Carpenter, T. Lauritsen, J. L. Harker, W. B. Walters, B. M. S. Amro, and P. Copp, Phys. Lett. B **771**, 119 (2017).
[26] V. V. Desai, W. Loveland, R. Yanez, G. Lane, S. Zhu, A. D. Ayangekaa, J. P. Greene, F. G. Kondev, R. V. F. Janssens, and P. A. Copp, Eur. Phys. J. A **56**, 150 (2020).
[27] V. V. Desai, A. Pica, W. Loveland, J. S. Barrett, E. A. McCutchan, S. Zhu, A. D. Ayangeakaa, M. P. Carpenter, J. P. Greene, T. Lauritsen, R. V. F. Janssens, B. M. S. Amro, and W. B. Walters, Phys. Rev. C **101**, 034612 (2020).
[28] Y. X. Watanabe, Y. H. Kim, S. C. Jeong, Y. Hirayama, N. Imai, H. Ishiyama, H. S. Jung, H. Miyatake, S. Choi, J. S. Song, E. Clement, G. de France, A. Navin, M. Rejmund, C. Schmitt, G. Pollarolo, L. Corradi, E. Fioretto, D. Montanari, M. Niikura *et al.*, Phys. Rev. Lett. **115**, 172503 (2015).
[29] C. Golabek, A. C. C. Villari, S. Heinz, W. Mittig, S. Bhattacharyya, D. Boilley, G. De France, A. Drouart, L. Gaudefroy, L. Giot, A. Marchix, V. Maslov, M. Morjean, G. Mukherjee, A. Navin, Y. Penionzkevich, F. Rejmund, M. Rejmund, P. Roussel-Chomaz, and C. Stodel, Int. J. Mod. Phys. E **17**, 2235 (2008).
[30] C. Golabek, S. Heinz, W. Mittig, F. Rejmund, A. C. C. Villari, S. Bhattacharyya, D. Boilley, G. De France, A. Drouart, L. Gaudefroy, L. Giot, V. Maslov, M. Morjean, G. Mukherjee, Y. Penionzkevich, P. Roussel-Chomaz, and C. Stodel, Eur. Phys. J. A **43**, 251 (2010).
[31] J. V. Kratz, M. Schädel, and H. W. Gäggeler, Phys. Rev. C **88**, 054615 (2013).
[32] M. Barbui, K. Hagel, J. B. Natowitz, A. Bonasera, R. Wada, P. K. Sahu, T. Materna, Z. Chen, L. Quin, G. A. Souliotis, G. Chubaryan, D. Fabris, M. Lunardon, M. Morando, S. Moretto,

G. Nebbia, S. Pesente, G. Viesti, F. Bocci, M. Cinausero *et al.*, J. Phys.: Conf. Ser. **312**, 082012 (2011).
[33] Z. Majka, M. Barbui, F. Becchetti, G. Chubaryan, D. Fabris, G. Giuliani, H. Griffin, K. Hagel, J. Kallunkathariyil, E. J. Kim, S. Kowalski, P. Lasko, T. Materna, S. Moretto, R. Murthy, G. Nebbia, T. O'Donnel, S. Pesente, G. Prete, L. Quin *et al.*, Acta Phys. Pol., B **45**, 279 (2014).
[34] A. Wieloch, M. Adamczyk, M. Barbui, N. Blando, G. Giuliani, K. Hagel, E. J. Kim, S. Kowalski, Z. Majka, J. Natowitz, K. Pelczar, R. Planeta, K. Schmidt, Z. Sosin, S. Wuenschel, K. Zelga, and H. Zheng, EPJ Web Conf. **117**, 01003 (2016).
[35] S. Wuenschel, K. Hagel, M. Barbui, J. Gauthier, X. G. Cao, R. Wada, E. J. Kim, Z. Majka, R. Płaneta, Z. Sosin, A. Wieloch, K. Zelga, S. Kowalski, K. Schmidt, C. Ma, G. Zhang, and J. B. Natowitz, Phys. Rev. C **97**, 064602 (2018).
[36] A. Winther, Nucl. Phys. A **572**, 191 (1994).
[37] A. Winther, Nucl. Phys. A **594**, 203 (1995).
[38] V. Volkov, Phys. Rep. **44**, 93 (1978).
[39] G. G. Adamian, N. V. Antonenko, R. V. Jolos, and W. Scheid, Nucl. Phys. A **619**, 241 (1997).
[40] G. G. Adamian, N. V. Antonenko, and D. Lacroix, Phys. Rev. C **82**, 064611 (2010).
[41] M. H. Mun, K. Kwak, G. G. Adamian, and N. V. Antonenko, Phys. Rev. C **101**, 044602 (2020).
[42] Z. Q. Feng, Phys. Rev. C **95**, 024615 (2017).
[43] X. J. Bao, S. Q. Guo, and P. H. Chen, Phys. Rev. C **105**, 024610 (2022).
[44] J. J. Li, N. Tang, Y. H. Zhang, X. R. Zhang, G. Zhang, and F. S. Zhang, Phys. Rev. C **106**, 014606 (2022).
[45] G. Zhang, J. J. Li, X. R. Zhang, B. Li, C. A. T. Sokhna, C. Wang, Z. Liu, and F. S. Zhang, Phys. Rev. C **102**, 024617 (2020).
[46] X. R. Zhang, G. Zhang, J. J. Li, S. H. Cheng, Z. Liu, and F. S. Zhang, Phys. Rev. C **103**, 024608 (2021).
[47] L. Zhu, J. Su, C. Li, and F. S. Zhang, Phys. Lett. B **829**, 137113 (2022).
[48] L. Zhu and J. Su, Phys. Rev. C **104**, 044606 (2021).
[49] N. Tang, X. R. Zhang, J. J. Li, P. W. Wen, and F. S. Zhang, Phys. Rev. C **106**, 034601 (2022).
[50] V. I. Zagrebaev and W. Greiner, Phys. Rev. Lett. **101**, 122701 (2008).
[51] V. I. Zagrebaev and W. Greiner, Phys. Rev. C **83**, 044618 (2011).
[52] V. I. Zagrebaev and W. Greiner, Phys. Rev. C **87**, 034608 (2013).
[53] V. V. Saiko and A. V. Karpov, Phys. Rev. C **99**, 014613 (2019).
[54] Z. J. Wu, L. Guo, Z. Liu, and G. X. Peng, Phys. Lett. B **825**, 136886 (2022).
[55] Z. J. Wu and L. Guo, Sci. China: Phys., Mech. Astron. **63**, 242021 (2020).
[56] K. Sekizawa, Front. Phys. **7**, 20 (2019).
[57] B. J. Roy, S. Santra, A. Pal, H. Kumawat, S. K. Pandit, V. V. Parkar, K. Ramachandran, K. Mahata, and K. Sekizawa, Phys. Rev. C **105**, 044611 (2022).
[58] A. S. Umar, V. E. Oberacker, and C. Simenel, Phys. Rev. C **92**, 024621 (2015).
[59] C. Simenel and A. S. Umar, Prog. Part. Nucl. Phys. **103**, 19 (2018).
[60] K. Godbey, C. Simenel, and A. S. Umar, Phys. Rev. C **101**, 034602 (2020).
[61] K. Zhao, Z. Liu, F. S. Zhang, and N. Wang, Phys. Lett. B **815**, 136101 (2021).
[62] K. Zhao, Z. X. Li, X. Z. Wu, and Y. X. Zhang, Phys. Rev. C **88**, 044605 (2013).
[63] C. Li, P. W. Wen, J. J. Li, G. Zhang, B. Li, X. X. Xu, Z. Liu, S. F. Zhu, and F. S. Zhang, Phys. Lett. B **776**, 278 (2018).
[64] C. Li, J. L. Tian, and F. S. Zhang, Phys. Lett. B **809**, 135697 (2020).
[65] C. Li, F. Zhang, J. J. Li, L. Zhu, J. L. Tian, N. Wang, and F. S. Zhang, Phys. Rev. C **93**, 014618 (2016).
[66] S. Ayik, B. Yilmaz, O. Yilmaz, and A. S. Umar, Phys. Rev. C **102**, 024619 (2020).
[67] S. Ayik, M. Arik, E. C. Karanfil, O. Yilmaz, B. Yilmaz, and A. S. Umar, Phys. Rev. C **104**, 054614 (2021).
[68] S. Ayik, M. Arik, O. Yilmaz, B. Yilmaz, and A. S. Umar, Phys. Rev. C **107**, 014609 (2023).
[69] A. K. Nasirov, G. Giardina, G. Mandaglio, M. Manganaro, F. Hanappe, S. Heinz, S. Hofmann, A. I. Muminov, and W. Scheid, Phys. Rev. C **79**, 024606 (2009).
[70] A. K. Nasirov, K. Kim, G. Mandaglio, G. Giardina, A. Muminov, and Y. Kim, Eur. Phys. J. A **49**, 147 (2013).
[71] G. Adamian, N. Antonenko, A. Diaz-Torres, and S. Heinz, Eur. Phys. J. A **56**, 47 (2020).
[72] G. Adamian and N. Antonenko, Eur. Phys. J. A **58**, 111 (2022).
[73] F. S. Zhang, Y. H. Zhang, M. H. Zhang, N. Tang, S. H. Cheng, J. J. Li, and W. Cheng, J. Beijing Norm. Univ.(Nat. Sci.) **58**, 392 (2022).
[74] L. Zhu, C. Li, C. C. Guo, J. Su, P. W. Wen, G. Zhang, and F. S. Zhang, Int. J. Mod. Phys. E **29**, 2030004 (2020).
[75] Y. H. Zhang, G. Zhang, J. J. Li, W. Cheng, and F. S. Zhang, J. Isot. **35**, 104 (2022).
[76] G. Adamian, N. Antonenko, and W. Scheid, Nucl. Phys. A **618**, 176 (1997).
[77] Z. Q. Feng, G. M. Jin, J. Q. Li, and W. Scheid, Phys. Rev. C **76**, 044606 (2007).
[78] P. Moller, J. Nix, W. Myers, and W. Swiatecki, At. Data Nucl. Data Tables **59**, 185 (1995).
[79] C. Y. Wong, Phys. Rev. Lett. **31**, 766 (1973).
[80] S. Ayik, B. Schürmann, and W. Nörenberg, Z. Phys. A: At. Nucl. (1975) **277**, 299 (1976).
[81] J. Li, X. Tang, and G. Wolschin, Phys. Lett. B **105**, 107 (1981).
[82] A. Nasirov, A. Fukushima, Y. Toyoshima, Y. Aritomo, A. Muminov, S. Kalandarov, and R. Utamuratov, Nucl. Phys. A **759**, 342 (2005).
[83] Z. Q. Feng, G. M. Jin, F. Fu, and J. Q. Li, Nucl. Phys. A **771**, 50 (2006).
[84] R. J. Charity, Phys. Rev. C **82**, 014610 (2010).
[85] D. Mancusi, R. J. Charity, and J. Cugnon, Phys. Rev. C **82**, 044610 (2010).
[86] K. E. Gregorich, K. J. Moody, D. Lee, W. K. Kot, R. B. Welch, P. A. Wilmarth, and G. T. Seaborg, Phys. Rev. C **35**, 2117 (1987).
[87] V. Zagrebaev and W. Greiner, J. Phys. G **34**, 2265 (2007).
[88] E. M. Kozulin, V. I. Zagrebaev, G. N. Knyazheva, I. M. Itkis, K. V. Novikov, M. G. Itkis, S. N. Dmitriev, I. M. Harca, A. E. Bondarchenko, A. V. Karpov, V. V. Saiko, and E. Vardaci, Phys. Rev. C **96**, 064621 (2017).
[89] R. Bass, Phys. Rev. Lett. **39**, 265 (1977).
[90] G. Wolschin and W. Nörenberg, Z. Phys. A: At. Nucl. (1975) **284**, 209 (1978).